Use of C-Band frequencies for satellite navigation: benefits and drawbacks

Markus Irsigler · Günter W. Hein · Andreas Schmitz-Peiffer

Abstract Although not considered for the first generation of European Galileo satellites, the use of C-Band frequencies for navigation purposes may be taken into account for a future generation of Galileo. For this reason, a frequency band of 20 MHz bandwidth (5,010–5,030 MHz) has been allocated in the course of the World Radio Communications Conference 2000 held in Istanbul, Turkey. The use of C-Band navigation signals offers both advantages and drawbacks. One example is the ionospheric path delay which is inversely proportional to the (squared) carrier frequency and is therefore significantly smaller at C-Band. On the other hand, the use of C-Band frequencies results in increased attenuation effects such as free space loss or rainfall attenuation. It is therefore necessary to provide a detailed analysis of the effects of C-Band frequencies on the navigation process. In order to assess the feasibility of using C-Band frequencies, various aspects of signal propagation and satellite signal tracking at C-Band are examined in the context of this article. In particular, aspects like free space loss, atmospheric effects, foliage attenuation, code and carrier tracking performance, code noise, phase noise and multipath are discussed with respect to their performance at C-Band. In order to allow comparison with the current GPS system, the performance at C-Band is compared to the L-Band performance under similar or identical conditions. The results of this analysis will finally be discussed with respect to their impact on satellite payload and receiver design.

M. Irsigler (✉) · G. W. Hein
Institute of Geodesy and Navigation,
University FAF Munich, 85577 Neubiberg, Germany
E-mail: markus.irsigler@unibw-muenchen.de
Tel.: +49-89-60043552
Fax: +49-89-60043019

A. Schmitz-Peiffer
EADS Astrium GmbH, 81663 München, Germany

Introduction

A future C-Band signal could use the frequency band between 5,010 and 5,030 MHz (European Radio Communications Office 2000), offering a bandwidth of 20 MHz in a frequency band not yet overloaded by other signal sources. Small ionospheric effects at these high frequencies can also be considered as a benefit. However, the use of C-Band frequencies also offers some drawbacks. In this context, increased free space loss represents the most significant issue. Increased signal attenuation due to foliage attenuation and in case of heavy rain can also be considered as drawbacks.

The main intention of this article is to provide an analysis of the effects of C-Band frequencies on the navigation process and to assess the feasibility of future C-Band technology. For this purpose, the article examines various aspects of signal propagation and satellite signal tracking at C-Band. In order to allow comparison with the current GPS system, the performance at C-Band is compared to the L-Band performance under similar or identical conditions. The results of this analysis are finally discussed with respect to possible consequences for future satellite payload and the design of future C-Band receivers.

The signal parameters (GPS vs. C-Band Galileo) used for the following analyses are listed in Table 1. Unless otherwise stated, all computations, diagrams and tables are based on these parameters. Note that in contrast to the GPS ranging codes which consist of rectangular chips, the C-Band signal, as discussed within the framework of the study, makes use of the raised cosine (RC) pulse shaping scheme. The actual shape of a raised cosine chip is defined by the so-called roll-off factor. For the Galileo C-Band signal, a roll-off factor of 0.22 has been assumed (Ebner 2000).

Signal propagation

Free space loss

The received power P_R at the output of a user antenna can be expressed as a function of the satellite transmit power P_T, the antenna gains G_S (satellite antenna) and G_R (receiving antenna), the geometric range d between the satellite and the user and the carrier wavelength λ (Misra and Enge 2001):

Table 1
GPS and Galileo signal parameters

Signal parameters	GPS L1-C/A	GPS L1-P(Y)	Galileo C
f [MHz]	1575.42	1575.42	5019.86
λ [m]	0.19	0.19	0.06
Chipping rate [Mcps]	1.023	10.23	8.184
Chip length [m]	293.05	29.31	36.63
Data rate [bps]	50	50	150
Predet. int. time [s]	0.02	0.02	0.0067
Bandwidth [MHz]	2.046	20.46	20
Chip shape	RECT	RECT	RC

$$P_R = \frac{P_T G_S G_R}{(4\pi d)^2} \cdot \lambda^2 = \frac{P_T G_S G_R}{L} \qquad (1)$$

$L=(4\pi d/\lambda)^2$ is often referred to as free space loss or range spreading loss. Due to the permanent motion of the satellites, the geometric range d changes with time. As a result, the free space loss can be calculated as a function of the satellite's elevation E. Maximum values for L can be expected for an elevation of $E=0°$ (satellite rises), whereas minimum values occur for $E=90°$ (zenithal pass). The resulting free space loss is illustrated in Fig. 1 for the GPS L1 signal ($\lambda=0.19$ m) and a future Galileo C-Band signal ($\lambda=0.06$ m), assuming a mean Earth radius of R_E=6,371 km and a semi major axis of $a\approx29,994$ km (Galileo constellation).

As can be derived from Fig. 1, free space loss at C-Band is approximately 10 dB higher than at L-Band. As a result, a future C-Band signal will be ten times weaker at the input of a user antenna than a corresponding L-Band signal (assuming identical satellite transmit power). To

compensate for the increased free space loss at C-Band, the satellite transmit power will have to be increased by a factor of 10. Alternatively, the gain of the user antenna could be increased. Such approaches will be discussed later on.

Ionospheric path delay

Ionospheric path delay is inversely proportional to the squared carrier frequency and depends on the total electron content (TEC) along the signal path. In the case of range measurements (carrier observations), the ionospheric group delay (phase advance) can be computed as follows (Parkinson and Spilker 1996):

$$\Delta s = +(-)\frac{40.31}{f^2} \cdot \text{TEC} \qquad (2)$$

Due to the constantly varying ionospheric conditions, the ionospheric path delay not only depends on the carrier frequency but also on the moment of observation (due to day/night variations, seasonal variations, current solar activity) and on the current location (geomagnetic latitude). The TEC values listed in Table 2 represent different ionospheric conditions (see e.g. Parkinson and Spilker 1996).

Figure 2 illustrates the resulting ranging errors subject to the carrier frequency. In order to consider different degrees of ionization, the computations were based on different TEC values. The gray band represents a ionospheric state of "normal" ionization (due to daytime/nighttime variations).

As can be derived from Fig. 2, ionospheric ranging errors can be significantly reduced by using C-Band frequencies. This aspect can be verified by Table 2,
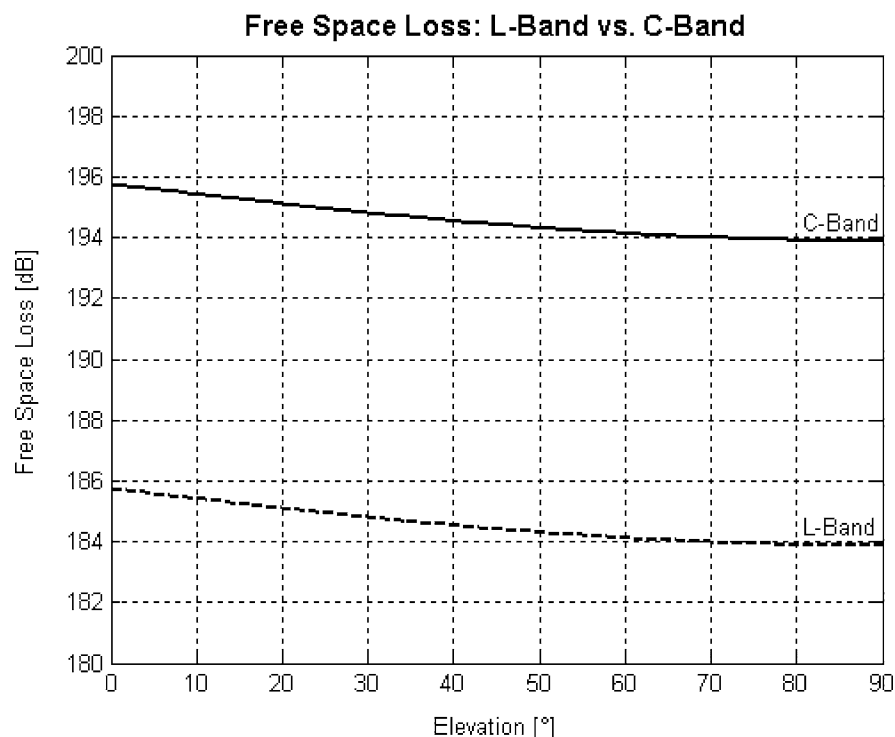

Fig. 1
Free space loss at L- and at C-Band

Table 2
Comparison of ionospheric ranging errors (L-Band vs. C-Band)

TEC [1/m^2]	$L2$ (m)	$L1$ (m)	C (m)
1×10^{16} (minimum)	0.27	0.16	0.02
5×10^{16} (nighttime)	1.34	0.81	0.08
5×10^{17} (daytime)	13.37	8.12	0.80
1×10^{18}	26.75	16.24	1.60
5×10^{18}	133.74	81.20	8.00
1×10^{19} (worst case)	267.42	162.41	16.00

where the resulting ranging errors are listed for the GPS $L1$ signal (f=1,575.42 MHz), the GPS $L2$ signal (f=1,227.6 MHz) and a future C-Band signal (f=5,019 MHz). Additionally, different ionospheric conditions are taken into account.

Ionospheric ranging errors at C-Band can be reduced by approximately a factor of 10 compared to $L1$ and almost a factor of 17 compared to $L2$. Note that in the case of "normal" ionospheric conditions (TEC $\leq 5\times10^{17}$ 1/m^2), the resulting ranging error at C-Band is less than 1 m. However, if higher values of TEC are assumed, the resulting ranging error can be much larger. Thus, even at C-Band, it will be necessary to provide a suitable ionospheric model or to carry out dual-frequency measurements to compensate for the ionospheric ranging error.

Ionospheric scintillation

The relationship of standard deviations of signal power variations and phase variations relative to that at $L1$ are

$$S_4(f) = S_4(L1)\left(\frac{f_{L1}}{f}\right)^{1.5} \tag{3}$$

and

$$\sigma_\phi(f) = \sigma_\phi(L1)\frac{f_{L1}}{f}, \tag{4}$$

respectively (Van Dierendonck et al. 1993), where S_4 is a measure of the power fade depth and frequency. Insertion of the two carrier frequencies leads to the result that amplitude scintillation fading is about 5.7 times less at C-Band than at L-Band and that phase scintillation variations are 3.2 times less. These variations are independent of platform dynamics, so that neither scintillation effect should present a tracking problem at C-Band.

Tropospheric path delay

The rainless troposphere is non-dispersive for frequencies below approximately 30 GHz. Therefore, the tropospheric path delay is identical for L-Band and C-Band signals. Tropospheric ranging errors vary between ∼2 m near zenith and up to 25 m at low elevation angles (Parkinson and Spilker 1996).

Attenuation due to water vapor and oxygen

Signal attenuation due to water vapor and oxygen is a function of the carrier frequency and the water vapor content of the lower atmosphere (ITU-R 1994). Figure 3 illustrates the zenithal attenuation subject to different carrier frequencies and different water vapor contents (the attenuation due to oxygen can be considered as constant for the frequency range illustrated in Fig. 3). Furthermore, attenuation due to water vapor and oxygen depends on the actual signal elevation. A worst case analysis for a signal elevation of E=10°, a (maximum) water vapor content of 30 g/cm^3 and rainy weather
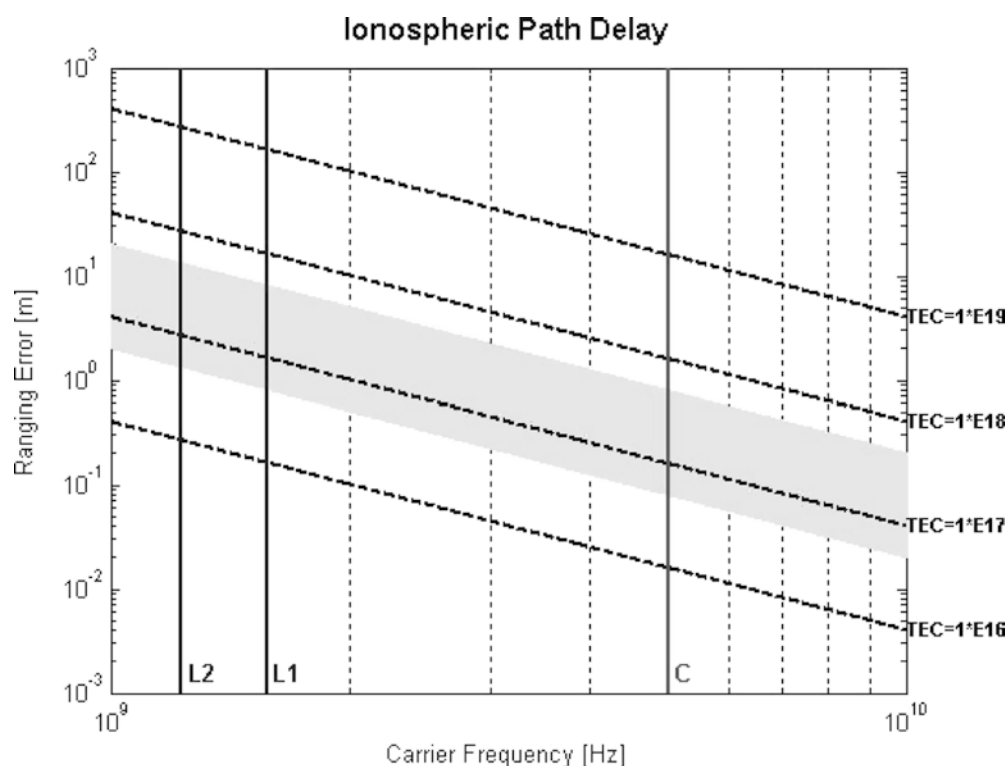

Fig. 2
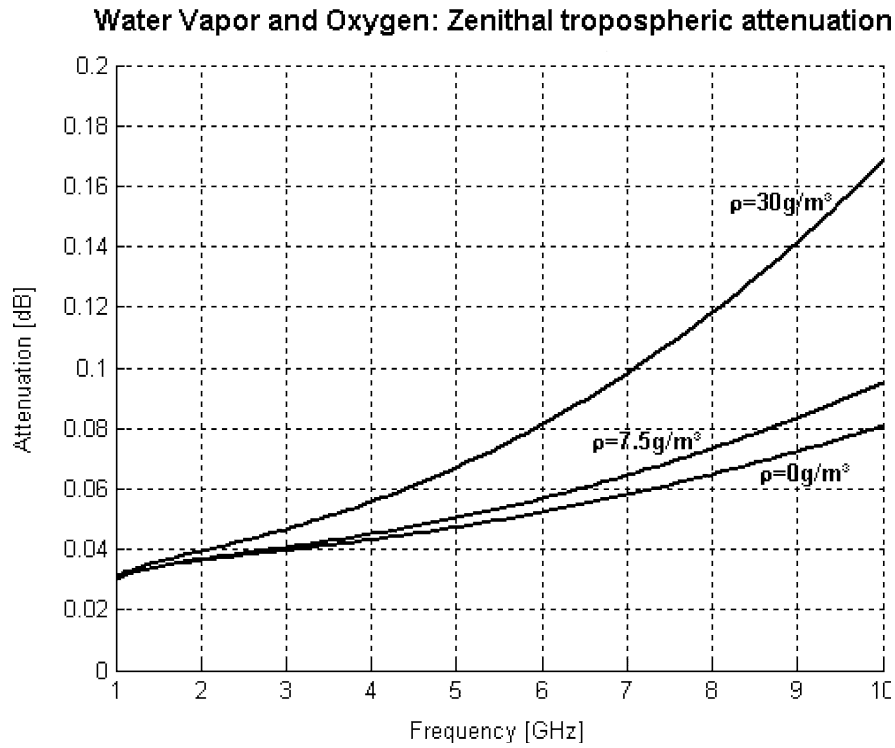Ionospheric ranging error subject to different carrier frequencies

Water Vapor and Oxygen: Zenithal tropospheric attenuation

Fig. 3
Zenithal tropospheric attenuation due to water vapor and oxygen as a function of the carrier frequency

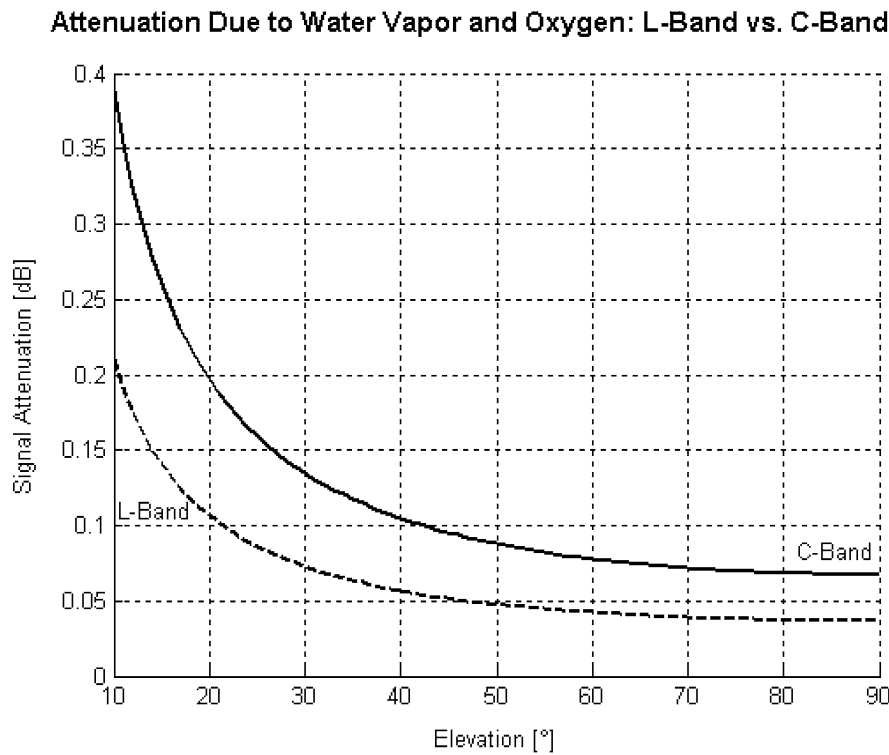## Attenuation Due to Water Vapor and Oxygen: L-Band vs. C-Band

Fig. 4
Worst case signal attenuation due to water vapor and oxygen at $L1$ (*dashed line*) and at C-Band (*solid line*)

conditions (equivalent height for water vapor: h_{w0}=2.1 km) leads to maximum attenuation values of 0.2 dB at $L1$ and 0.4 dB at C-Band (see Fig. 4).

Rainfall attenuation

Rainfall attenuation at C-Band has been computed on the basis of the ITU-R rainfall model which can be found in Maral and Bousquet (1999). The input parameters are:

– Carrier frequency.
– Actual amount of rainfall and length of signal path through the rain. In the case of the ITU-R rainfall model, the world is divided into dedicated zones, each of them representing a region with a dedicated statis-

tical amount of rainfall (based on an availability of 99.99%).

– Height of user above mean sea level.
– Upper rainfall limit (mean height of the 0° isotherm in case of rainfall). To define this height, several models (regional or global) can be used. In all models, the upper rainfall limit is a function of the user's geographic latitude.
– Signal elevation and availability.

In order to compute worst case attenuation values, the following assumptions have been made:

– Tropical thunderstorm with maximum statistical amount of rainfall. This implies the selection of zone P with a statistical amount of rainfall of $R_{0.01}$=145 mm/h.
– The user is assumed to be at mean sea level.
– The signal elevation is set to E=90°.
– A global rainfall model with an upper rainfall limit of 5 km is assumed.
– Availability a=99.999%.

Based on these assumptions, the resulting attenuation was computed for L- and C-Band frequencies. At L-Band, the resulting attenuation is $\sim$0.1 dB and is thus negligible. At C-Band, however, values up to 4.6 dB can occur. The main results are summarized in Fig. 5 and Table 3.

Attenuation due to clouds and fog

Signal attenuation due to clouds and fog depends on the carrier frequency, the liquid water content and on the spatial distribution of the clouds (Liebe 1989). Assuming a cumulonimbus (thundercloud) of 10 km vertical and horizontal extent and a water content of 3 g/m³, the worst

case signal attenuation for L- and C-Band frequencies is approximately 0.1 dB at L-Band and 0.9 dB at C-Band.

Tropospheric scintillation

Figure 6 illustrates the annual cumulative distributions of fade depths due to tropospheric scintillation at C-Band (5.02 GHz) for high wet refractivity at the Earth's surface (tropical regions, N_{wet}=114) and elevation angles between 5 and 30°. The analysis is based on the corresponding ITU-R model (ITU-R 1994). According to this model, amplitude scintillation at C-Band (fade depths in dB) is about two times higher than at L-Band. Figure 6 shows that for low elevation angles and short periods of time, signal attenuation due to tropospheric scintillation can be of concern. Range fluctuations σ_R (RMS) due to tropospheric scintillation reach a maximum of 7.5 mm (worst case at E=5°) (Millman 1970) and do not depend on the carrier frequency. They decrease with higher elevation angles. The corresponding phase fluctuations σ_{ph} depend on the wavelength λ and can be expressed by $\sigma_{PH}=\sigma_R(360°/\lambda)$. As a result, the resulting worst case phase fluctuations at 5° elevation angle are 45° at C-Band and 14° at L-Band.

Foliage attenuation

Foliage attenuation can be computed by means of several, mostly empirical models (e.g. Goldhirsch and Vogel 1998 and Kajiwara 2000). A major problem is that such models either do not consider different types and densities of foliage or that L-Band attenuation values must be extrapolated to C-Band. Nevertheless, the influence of foliage attenuation can be roughly estimated by means of such models. As a result, average attenuation values of $\sim$1 dB/m at L-Band and $\sim$2 dB/m at C-Band must be expected.
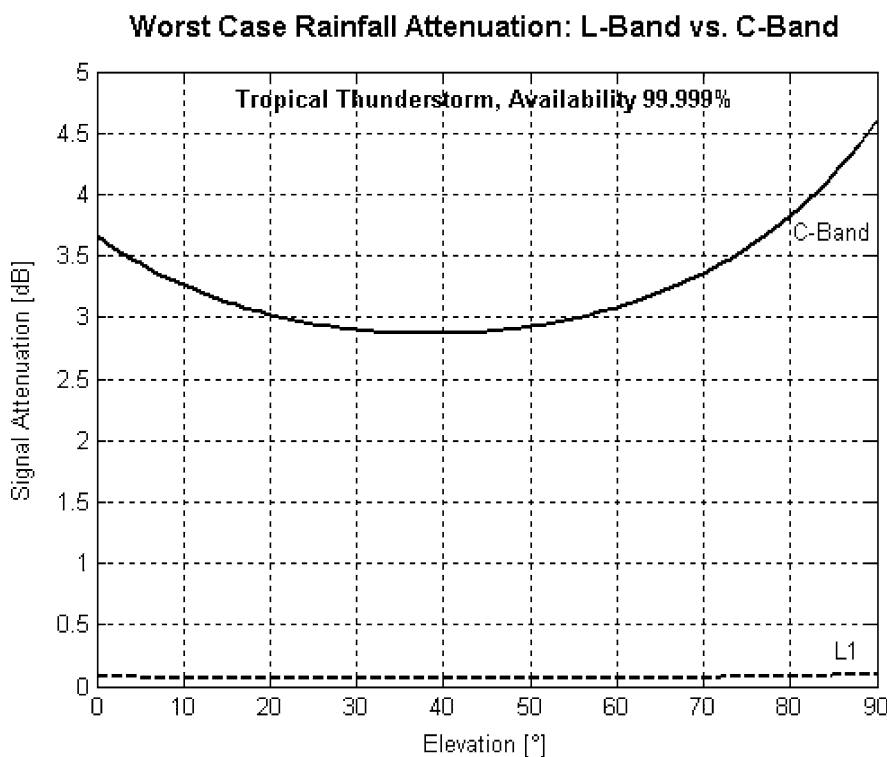

Fig. 5
Worst case rainfall attenuation at L- and at C-Band

Table 3
Rainfall attenuation for GPS $L1$ and a future C-Band signal

$p\%$	Availability (%)	Rainfall attenuation @ $E=90°$	
		$L1$ (dB)	C (dB)
1	99	0.006	0.26
0.1	99.9	0.018	0.82
0.01	99.99	0.046	2.15
0.001	99.999	0.098	4.61

Table 4
Signal propagation at L- and at C-Band

Parameter	L	C	Factor
Free space loss	+	−	10
Ionospheric path delay	−	+	10
Ionospheric amplitude scintillation	−	+	5.6
Ionospheric phase scintillation	−	+	3.1
Ionospheric refraction	−	+	10
Ionospheric Doppler shift	−	+	3
Tropospheric path delay	o	o	–
Tropospheric amplitude scintillation	+	−	2
Tropospheric phase scintillation	+	−	3
Water vapor and oxygen (worst case)	+	−	0.2 dB
Rainfall attenuation (worst case)	+	−	4.5 dB
Clouds and fog (worst case)	+	−	0.8 dB
Foliage attenuation	+	−	1 dB/m

However, these values may strongly vary subject to foliage types and densities.

Summary

Table 4 summarizes the different signal propagation characteristics at L- and at C-Band. Benefits with respect to the other frequency band are indicated by "+" whereas drawbacks are indicated by "−". The quantitative difference between the two frequency bands are listed in column 3. Although not discussed above, the "performance" of ionospheric refraction and ionospheric Doppler shift at L- and at C-Band is also listed in Table 4.

Signal tracking

The most important signal tracking approaches inside a satellite receiver are the delay lock loop (DLL) and the phase lock loop (PLL). The DLL aligns the incoming code with an identical code generated by the receiver, whereas the PLL aligns the phase of the received signal with that of the receiver-generated reference signal. The following sections provide an analysis of the Doppler shifts which must be expected at C-Band and examine whether or not robust code and carrier tracking can be achieved at C-Band. This analysis determines the parameters for which the code or carrier tracking loop loses lock. Note, however, that loss-of-lock is generally a non-deterministic, statistical effect and that an analysis of the actual tracking performance is generally a nonlinear problem. Within the scope of this article, tracking performance will be treated as a linear problem.
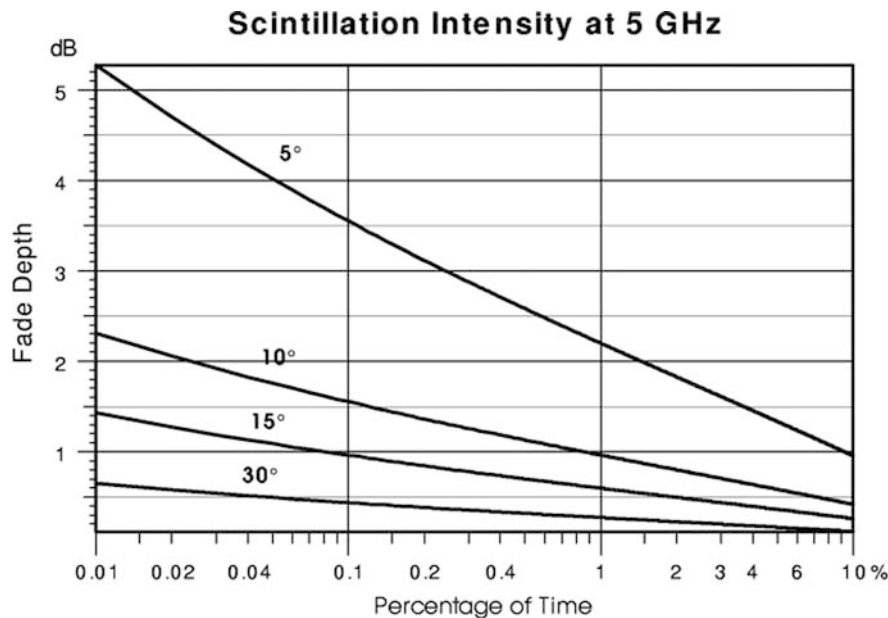

Fig. 6
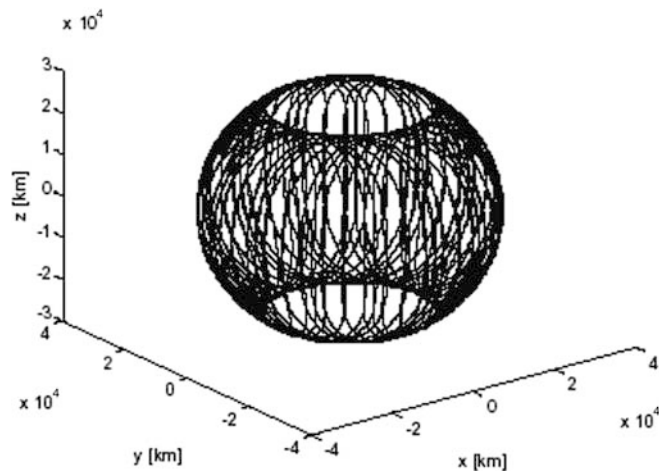Cumulative distribution of tropospheric amplitude scintillation at C-Band

Fig. 7
Three-dimensional configuration of the 30 GalileoSat orbits in an ECEF coordination system

Galileo Doppler shifts

In general, multiple satellite signals are received with different delays and Doppler frequency offsets. A satellite at zenith, for example, is at the point of closest approach and has no Doppler offset whereas a satellite on the horizon is at its maximum distance and exhibits maximum Doppler offset. For GPS, this potential range difference is 25,738−20,183 km=5,600.9 km, resulting in a 18.68 ms delay difference. In addition, the satellite on the horizon has a radial velocity that is positive or negative. In the case of the GPS, the maximum Doppler shifts of the satellite signals on ground can reach up to ±6 kHz. As the carrier frequency for the C-Band is three times higher compared to the L-Band, a larger Doppler frequency shift can be expected for C-Band frequencies. The expected Doppler shifts at C-Band were determined by simulations.
Baseline for these simulations is the Galileo constellation which consists of 30 satellites moving in three planes

according to a Walker pattern 27/3/1, which means nine operating satellites and one spare per plane. The satellite period is 14.4 h and the repetition time of the constellation is 3 days. The in-orbit spares allow high service availability by fast satellite replacement, which typically lasts 1 week. The orbit height of the satellites is 23,616 km (medium earth orbit, MEO). A three-dimensional figure of the GalileoSat orbits over a 24 h period in the earth-centered, earth-fixed (ECEF) coordinate system is shown in Fig. 7. Due to the inclination of the satellite orbit and because the satellites will not move over the pole regions there will be a limited availability of the Galileo signal in space (SIS) over the northern and southern polar region.

A user on earth receives satellite signals with a Doppler frequency shift due to the fact that the satellite moves relative to the (perhaps also moving) user. With consideration of the time dilation for a moving geocentric coordination system (Lorentz-transformation), the frequency f' of the received satellite signal and the corresponding Doppler frequency shift is

$$f' = f\sqrt{\frac{1 - v_r/c}{1 + v_r/c}} \quad \text{and}$$

$$df' = f' - f = f\left(\sqrt{\frac{1 - v_r/c}{1 + v_r/c}} - 1\right), \tag{5}$$

respectively. f denotes the transmitting frequency, v_r the relative velocity between satellite and receiver and c the velocity of light.

Simulations. In order to calculate the Doppler frequency shifts at C-Band, the satellite constellation has been simulated over a period of 3 days using STK and MATLAB software. For the statistical analysis of the Doppler frequencies, 169 fixed observation points on the ground have been defined between 60° southern and 60° northern latitude, evenly spread with a distance of 7.5° in latitude (see Fig. 8). Due to the symmetry of the Galileo constellation
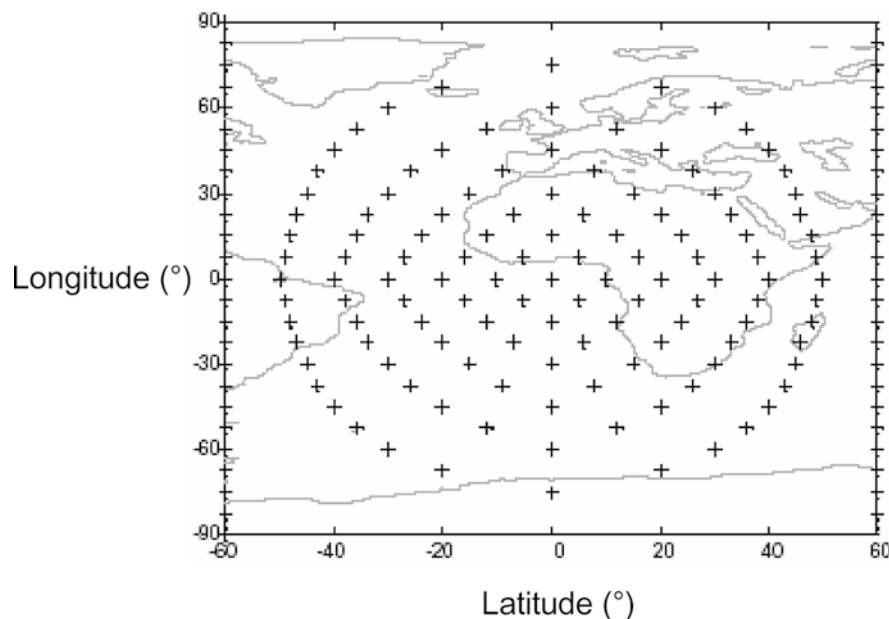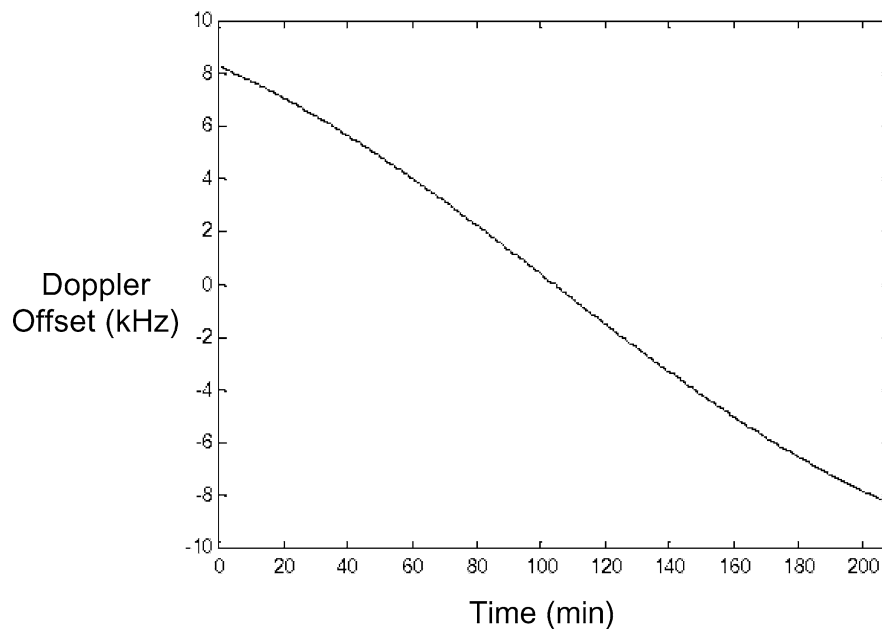

Fig. 8
User positions on ground

Table 5
Absolute value of the maximal Doppler-frequency shift for different
elevation masking angles

Minimum elevation mask (°)	Number of observation points	Absolute value of the maximum Doppler shift (kHz)
0	8615190	10.74
10	6922350	10.57
25	4440900	9.65

relative to the polar axis, a longitudinal sector of 120° is
sufficient. For each observation point B_j and sampling
instance the line-of-sight (LOS) distance r_{ij} to each satellite
i and its relative velocity v_r (derivation of the slant range
r_{ij}) is calculated. The calculation of the distances of the
satellites to the users considering constraints like elevation
masks between user and satellite, which block the Galileo
SIS (masking angle) and the determination of relative
velocity and Doppler frequency have been performed with
MATLAB.
A typical Doppler profile is shown in Fig. 9. The satellite is
visible for 3 h 27 min. The number of simulation values
depends on the size of the elevation masking angle. For
an elevation masking angle of 0° the total number of
observed Doppler values over the 3 day simulation per-
iod is 8645310. Table 5 shows the absolute value of the
maximum Doppler frequency shift. The higher the ele-
vation masking angle, the lower is the maximum of the
Doppler frequency offset, the lower is the impact of the
Doppler shift on the receiver. The maximum Doppler
offset in this specific Galileo simulation case reaches
10.74 kHz for an elevation masking angle of 0°. The
maximum frequency shifts are observed in the far
northern and southern latitudes between ±67.5° and
±90°. Relativistic effects are negligible, and so is the
impact of a moving receiver due to the Galileo MEO

constellation. However, in the case of a low earth orbit
(LEO) constellation, the impact of a moving receiver
would not be negligible and can dominate the satellite
Doppler shift.

DLL tracking performance
The code correlation process can be carried out by dif-
ferent types of discriminators and different correlation
techniques. As a result, each type of DLL will show slight
differences in tracking performance. According to Kaplan
(1996), the dominant sources of range error in a code
tracking loop are the thermal noise range error and the
dynamic stress error. The total sum of these error sources
must not exceed the rule-of-thumb tracking threshold that
can be defined by the following expression (Kaplan 1996):

$$\sigma_{DLL} = \sigma_T + \frac{e(t)}{3} \leq T_C \cdot \frac{d}{6} \ [m] \tag{6}$$

There, σ_T is the thermal noise, $e(t)$ the dynamic stress
error caused by signal dynamics, d the correlator spacing
between early and late code (d=1 for the standard corre-
lator, d=0.1 for the Narrow Correlator) and T_C the chip
length of the code. Note that the tracking threshold defined
by Eq. 6 is a rule-of-thumb threshold and does not hold for
all types of correlation techniques. Use of a standard
correlator or a Narrow Correlator, for example, leads to
tracking thresholds which are probably higher than indi-
cated. Nevertheless, Eq. 6 can serve as a starting point to
assess the DLL tracking performance as a first approxi-
mation. If the resulting DLL range error (thermal noise
plus one third of the dynamic stress error) exceeds the
rule-of-thumb tracking threshold defined by Eq. 6, the
satellite signal cannot be tracked properly (loss-of-lock).
Otherwise, if the total range error is less than this
threshold, the DLL can be considered as stable.
Assuming that an unaided first-order DLL with a
non-coherent early–late (E–L) discriminator is used, the

thermal noise and the dynamic stress error can be expressed as follows (Parkinson and Spilker 1996):

$$\sigma_T = T_C \cdot \sqrt{\frac{B_L \cdot d}{2 \cdot c/n_0} \left[1 + \frac{2}{(2-d) \cdot T \cdot c/n_0}\right]} \; [\text{m}] \qquad (7)$$

$$e_1(t) = \frac{\dot{x}(t)}{4B_L} \; [\text{m}] \qquad (8)$$

The influence of thermal noise depends on the carrier-to-noise power $c/n_0 = 10^{C/10N0}$ (C/N_0 expressed in [dB-Hz]), the chip length of code T_C [m], the pre-detection integration time T [s], the code loop noise bandwidth B_L [Hz] and the correlator spacing d. The dynamic stress error depends on the LOS signal dynamics and the code loop noise bandwidth B_L [Hz]. In case of a first-order loop, the DLL is sensitive to velocity stress, whereas second- and third-order DLLs are sensitive to acceleration and jerk stress, respectively.

Both error sources do not depend on the carrier frequency. As a result, there is no difference in DLL tracking performance between L-Band and C-Band (assuming identical signal structure and DLL design in both bands). This statement can be verified by Fig. 10. There, the total first-order DLL tracking error is plotted as a function of the actual C/N_0 and the LOS velocity. Additionally, the tracking threshold defined by Eq. 6 is plotted as a gray plane. The DLL can be deemed to be stable if the total tracking error is less than the tracking threshold, i.e. for all parts of the surface that lie below the gray plane. The following illustrations base on a correlator spacing of $d=1$ (Standard Correlator) and a loop noise bandwidth of $B_L=1$ Hz. Due to their similar code chip lengths, the (future) Galileo C-Band signal is compared with the current GPS P(Y)-Code. The analysis is based on the code chip lengths and pre-detection integration times listed in Table 1.

It is obvious that there are only little differences between GPS P(Y) and a Galileo C-Band signal. These differences

result from the differing code chip lengths and pre-detection integration times (not from the different carrier frequencies). Since the DLL performance does not depend on the carrier frequency, all current DLL technologies and implementations can be used at C-Band. Especially techniques like carrier aiding or tight coupling are also feasible at C-Band.

PLL tracking performance

According to Kaplan (1996) or Parkinson and Spilker (1996), the dominant error sources of a phase tracking loop are the thermal phase noise σ_T, the oscillator phase noise induced by frequency instabilities of the receiver and/or satellite clock ($\sigma_{A,Rec}$, $\sigma_{A,Sat}$), the vibration induced oscillator phase noise σ_{vib} and the dynamic stress error $e(t)$. The occurring error sources depend on the parameters listed in Table 6 and the PLL can be deemed to be stable if the following equation holds (e.g. Kaplan 1996):

$$\sigma_{PLL} = \sqrt{\sigma_T^2 + \sigma_{A,Rec}^2 + \sigma_{A,Sat}^2 + \sigma_V^2} + \frac{e(t)}{3} \le 15° \qquad (9)$$

Formulas for modeling the thermal noise jitter and the dynamic stress error as well as approaches for modeling oscillator phase noise and vibration induced phase noise can be found in Kaplan (1996) or Parkinson and Spilker (1996). A detailed analysis of PLL tracking performance, including models for all error sources can be found in Irsigler and Eissfeller (2002).

Oscillator phase noise, vibration induced phase noise and dynamic stress error are proportional to the carrier frequency. As a result, we can expect a significant increase of PLL jitter at C-Band. Thus, the PLL performance at C-Band should be much poorer than at L-Band. This statement can be verified by means of a PLL performance analysis which is based on the following assumptions:

- Non-coherent carrier tracking
- Second-order PLL
- Loop noise bandwidth: $B_L=15$ Hz
- Predetection integration times: see Table 1
- Carrier frequencies: see Table 1

Fig. 10
DLL tracking performance for the GPS P(Y)-Code (*left diagram*) and the Galileo C-Band signal (*right diagram*)
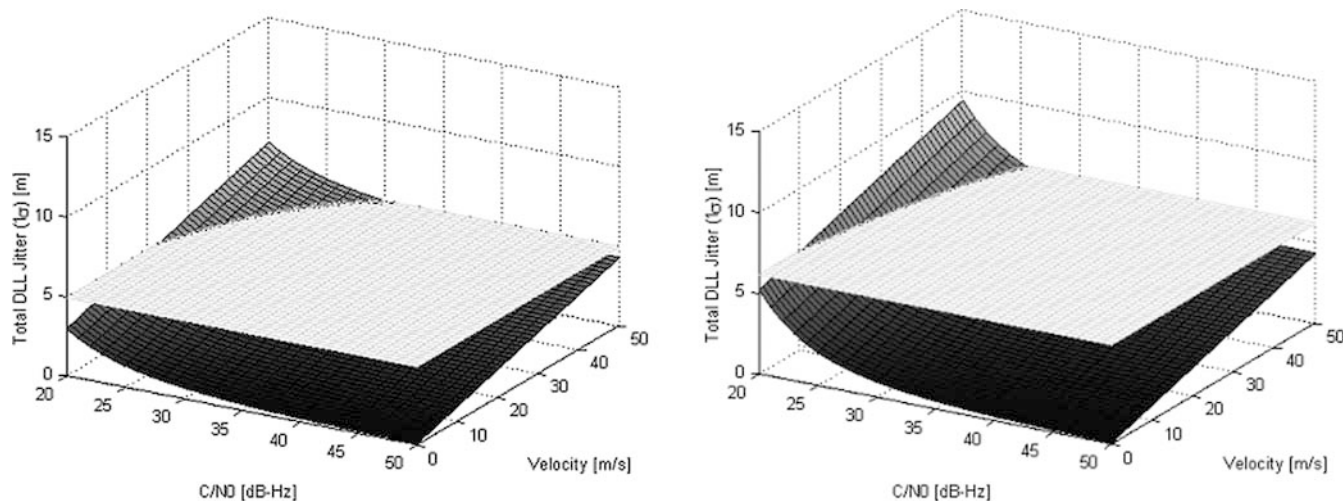
**Table 6**
Signal and loop parameters affecting the PLL error sources

Thermal noise	Loop noise bandwidth B_L
	Predetection integration time T
	C/N_0
Oscillator phase noise	Loop order
	Loop noise bandwidth B_L
	Clock parameters h_0, h_{-1}, h_{-2}
	Carrier frequency f
Vibration induced phase noise	Loop order
	Loop noise bandwidth B_L
	G-sensitivity of oscillator
	Power spectral density of vibration
	Carrier frequency f
Dynamic stress error	Loop order
	Loop noise bandwidth B_L
	Signal dynamics (LOS)
	Carrier frequency f

– Satellite clock: Rubidium
– Receiver oscillator: temperature compensated crystal oscillator (TCXO)
– Power spectral density (PSD) of vibration: 0.05 g²/Hz
– Frequency range of vibration: 25 Hz<f_{vib}<2,500 Hz.

The parameters that specify the influence of random vibration represent typical values for aircraft applications so that the total PLL jitter illustrated in Fig. 11 is a good representation for a dynamic application.

The result of this analysis shows a very poor PLL tracking performance at C-Band. Based on the aforementioned scenario, the total PLL jitter at C-Band is mostly higher than the tracking threshold defined by Eq. 10. Even in the case of only weak accelerations, the receiver will not be able to track the signal and even if several loop, clock or vibration parameters are modified, the PLL performance at C-Band is always much poorer than at L-Band. Possible approaches to enhance the poor PLL performance at C-Band are discussed later on.
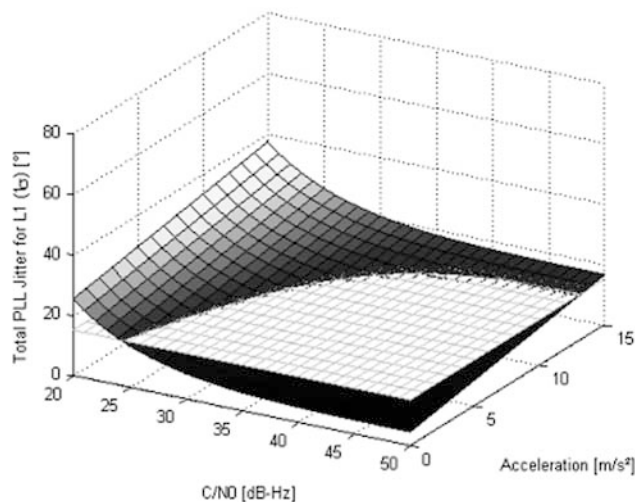
Code noise
To evaluate the code noise performance of a future C-Band signal, the well-known expressions of linear DLL analysis can be used. Assuming a non-coherent E–L discriminator, the thermal noise can be expressed as follows (Parkinson and Spilker 1996):

$$\sigma_T = T_C \cdot \sqrt{\frac{B_L \cdot d}{2 \cdot c/n_0} \left[1 + \frac{2}{(2-d) \cdot T \cdot c/n_0} \right]} \ [\text{m}] \qquad (10)$$

There, T_c [m] is the code chip length, T [s] the predetection integration time (corresponding with the inverse data rate), c/n_0 the carrier-to-noise ratio, d the chip spacing between early and late reference code and B_L [Hz] the loop noise bandwidth. Since the thermal noise error does not depend on the carrier frequency, there will be no difference between L-Band and C-Band noise performance if we assume identical signal structure (identical code chip length and data rate).
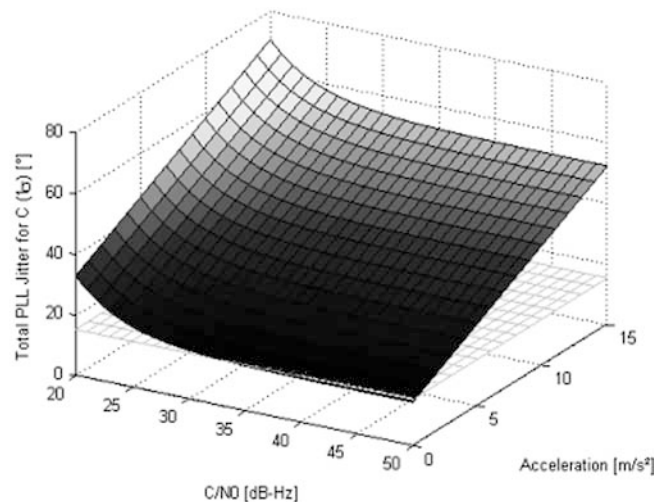
In the following, the code noise of the GPS-P(Y) signal will be compared to that of a future C-Band signal. For these purposes, a correlator spacing of d=1 is assumed (also called "standard" or "wide" correlation technique). The other relevant parameters (chip lengths, data rates, predetection integration times) for both signals can be found in Table 1. The resulting code noise is illustrated in Fig. 12 as a function of the code loop noise bandwidth. Furthermore, different values of C/N_0 are assumed.

The code noise of the C-Band signal is slightly higher than that of the L-Band GPS signal. This is caused by its slightly higher code chip length and the differing pre-detection integration times (not by the differing carrier frequencies). In practice, the expected code noise might be somewhat smaller because a more detailed analysis would require consideration of additional signal parameters like signal bandwidth and chip shaping.

Phase noise

Thermal noise
The linear PLL analysis provides the expression for the computation of thermal phase noise (Parkinson and Spilker 1996):

Fig. 11
Total PLL jitter for the GPS L1 signal (*upper diagram*) and a C-Band signal (*lower diagram*) as a function of C/N_0 and the signal dynamics (LOS acceleration)
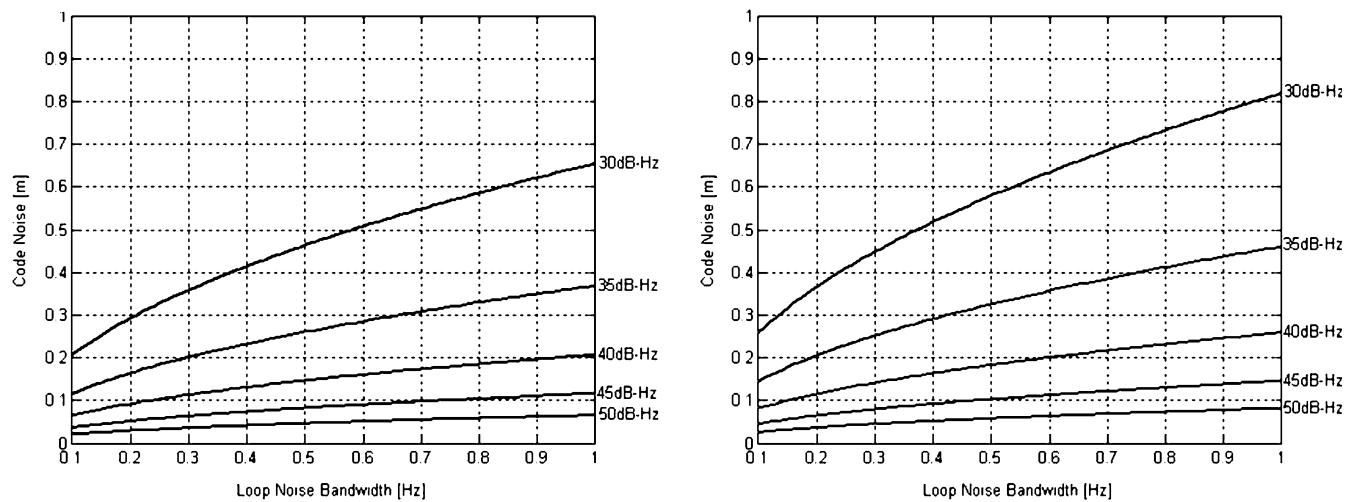
Fig. 12
Code noise performance of the GPS-P(Y) signal (*left diagram*) and a future C-Band signal (*right diagram*)
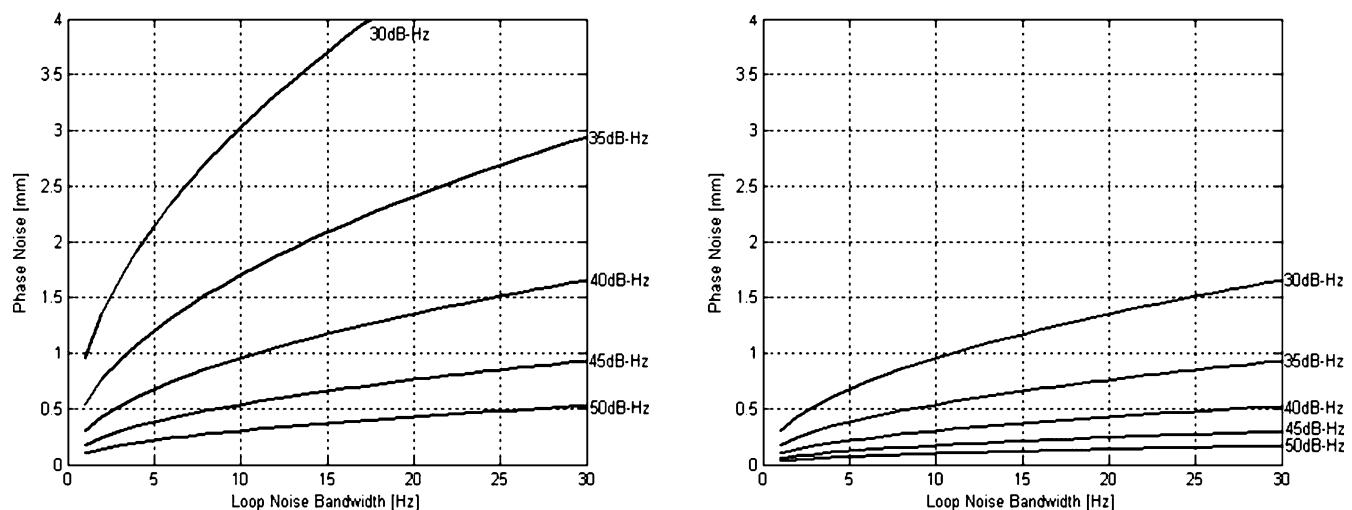
$$\sigma_T = \frac{\lambda}{2\pi} \sqrt{\frac{B_L}{c/n_0} \left[1 + \frac{1}{2T \cdot c/n_0}\right]} \ [m] \tag{11}$$

λ [m] is the carrier wave, T [s] the pre detection integration time (inverse data rate), c/n_0 is the carrier-to-noise ratio and B_L [Hz] the loop noise bandwidth. Since thermal noise is directly proportional to the carrier wavelength, its influence can be reduced by decrease of the carrier wavelength. As a result, the influence of thermal noise at C-Band is much less than at L-Band ($\sim$factor of 3). Figure 13 illustrates the thermal noise performance for the GPS L1 signal (λ=0.19 m) and the C-Band signal (λ=0.06 m) as a function of the loop noise bandwidth B_L. Again, the corresponding pre-detection integration times are listed in Table 1.

In case both signals have identical C/N_0, the influence of thermal phase noise can be significantly reduced by use of the C-Band frequency (by a factor of 3). If we assume identical transmit power in both bands, however, the C-Band signal will be 10–16 dB weaker than an equivalent L-Band signal (depending on the actual tropospheric attenuation). If this effect is taken into account, there will be no benefit for the C-Band signal. On the other hand, if the 10–16 dB power loss at C-Band can be compensated (e.g. by increase of the satellite transmit power or by use of phased array antennas) the phase noise performance will be much better than at L-Band.

Additional consideration of oscillator phase noise
In addition to thermal noise, the reference oscillator is a second source of phase jitter. Oscillator phase noise can be divided into noise induced by frequency instabilities (Allan deviation phase noise) and vibration-induced phase noise. While vibration-induced phase noise is only an issue for kinematic applications, Allan deviation phase noise is always present. It can be shown, however, that even if oscillator phase noise is considered, the resulting overall phase jitter at C-Band (thermal noise + oscillator phase noise) can also be significantly reduced (also by a factor of 3) compared to the L-Band (again assuming identical satellite
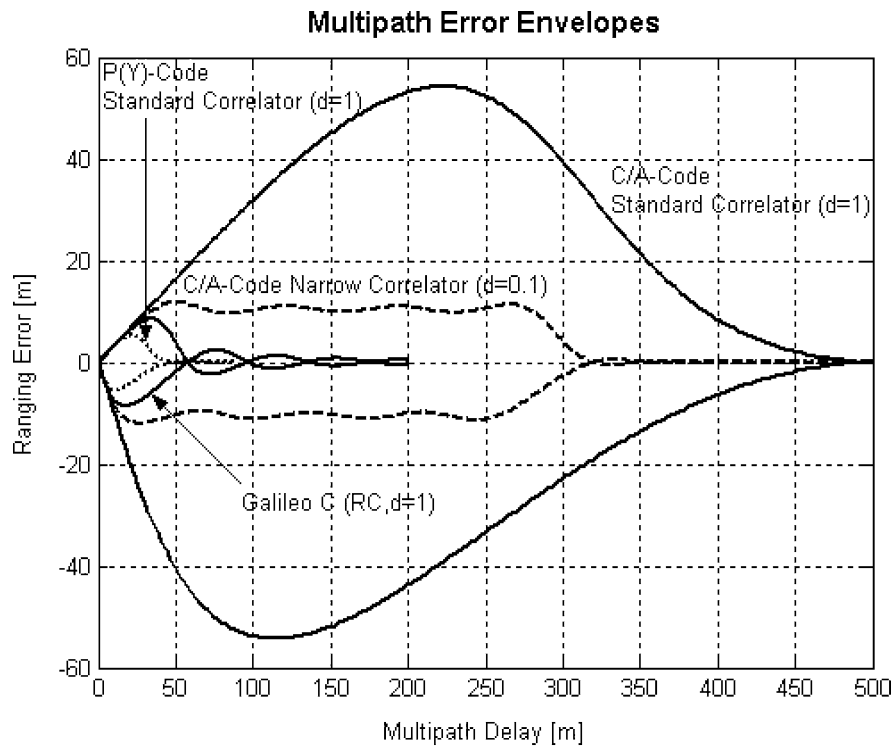
Fig. 13
Thermal phase noise performance for the GPS-L1 signal (*left diagram*) and the C-Band signal (*right diagram*)

Multipath Error Envelopes

Fig. 14
Ranging errors caused by multipath. Different signals as well as different types of correlators are considered
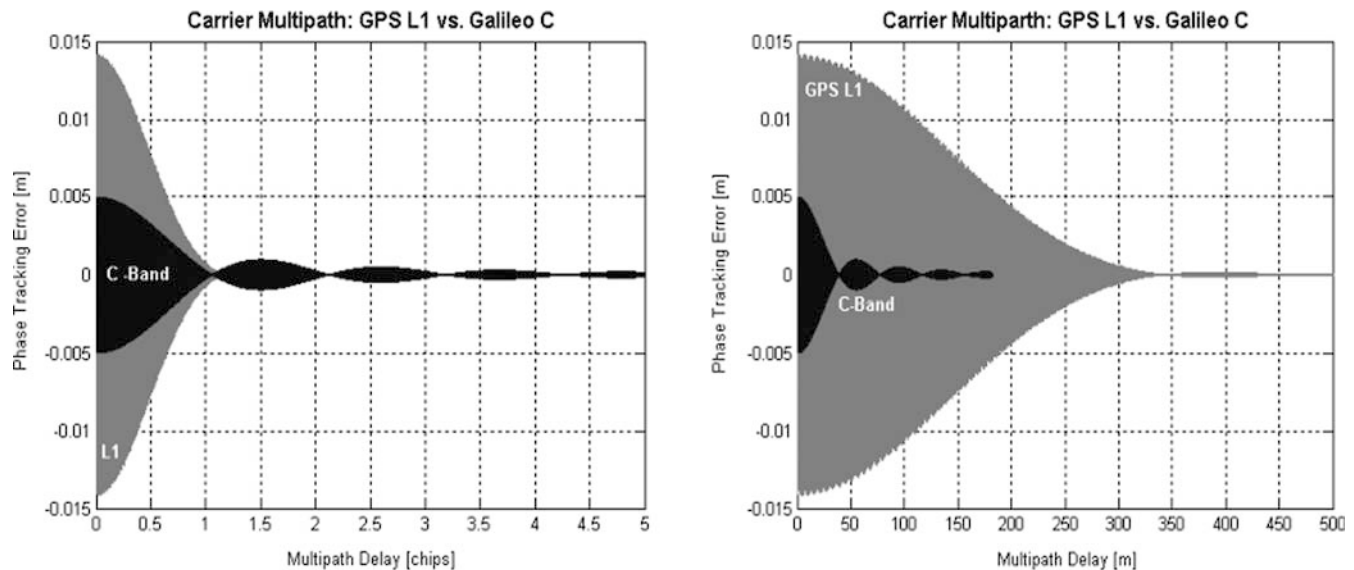

Fig. 15
Carrier multipath for the GPS L1 and the Galileo C-Band signal as a function of the geometric path delay expressed in [chips] (*left diagram*) and as a function of the geometric path delay expressed in [m] (*right diagram*)

transmit power). However, as it is the case for thermal noise, the gain in phase tracking accuracy at C-Band is compensated by the significantly lower C/N_0. If uncompensated, there will again be no benefit for the C-Band signal.

Multipath performance
In the case of multipath, not only is the LOS component of the satellite signal received but also at least one additional component reflected by objects in the vicinity of the receiver. The total sum of all incoming signal components is processed by the receiver resulting in ranging and positioning errors.

Code multipath
This form of multipath results in ranging errors which mainly depend on the code chip length T_C, the correlator spacing d (E–L) and the geometric path delay. Additionally, parameters like signal bandwidth and pulse shape have to be considered. Figure 14 illustrates the resulting ranging errors for different satellite signals and correlation techniques. The analysis is based on the following assumptions (see Table 1 for details):
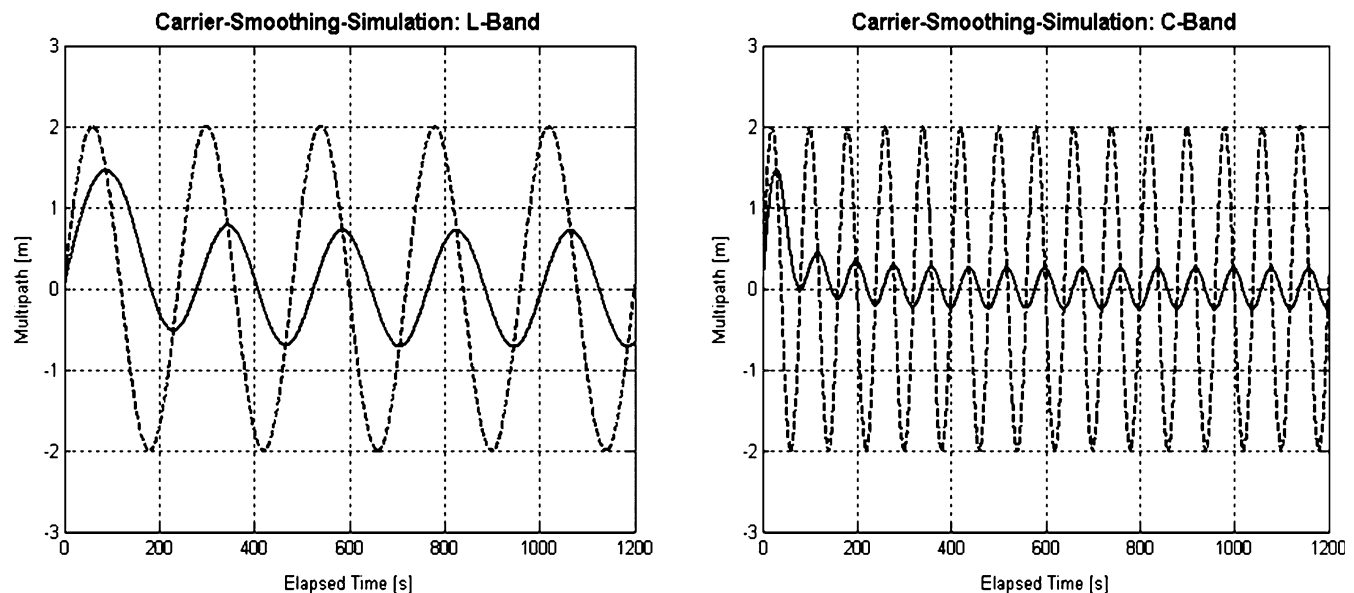
Fig. 16
Efficiency of multipath reduction by using the carrier smoothing process at L-Band (*left diagram*) and at C-Band (*right diagram*). The original multipath variations are indicated as *dashed lines*, whereas the smoothed multipath variations are illustrated as *solid lines*. Identical smoothing constants were used at both frequency bands

− LOS signal available (no shadowing effects)
− One single multipath signal
− Attenuation factor: $\alpha=0.5$
− Tested signals: GPS C/A and P(Y) ($d=1$), GPS C/A ($d=0.1$)[1] and Galileo C ($d=1$).

Ranging errors caused by code multipath do not depend on the carrier frequency. As a result, the resulting ranging errors would be the same at L- and at C-Band if identical signal structures, identical attenuation factors, correlation techniques and signal bandwidths were assumed. Assuming identical correlation techniques and signal bandwidths, the maximum ranging error and the maximum multipath delay that affects range measurements only depend on the code chip length. Due to similar code chip lengths, the multipath performance for the C-Band signal is similar to those of the GPS P(Y) signal.

Carrier multipath

The overlay of several multipath signal components may also result in phase errors. Such errors θ depend on the amount i of reflected signal components, their corresponding attenuation α_i and the phase offsets ϕ_i of the signal components with respect to the LOS signal component (multipath relative phase). If only one multipath signal is considered, the resulting phase error θ can be expressed by the ArcTangent detector function (e.g. Parkinson and Spilker 1996)

$$\tan \theta = \frac{\alpha R(\tau - \delta) \sin \phi}{R(\tau) + \alpha R(\tau - \delta) \cos \phi}, \tag{12}$$

---

[1]Narrow Correlator (Van Dierendonck et al. 1992), $B_W=8$ MHz

where the multipath relative phase is related to the geometric path delay d and the carrier wavelength λ (both expressed in [m]) via

$$\phi = \frac{2\pi d}{\lambda}. \tag{13}$$

According to Eq. 12, the multipath error θ depends on the multipath relative amplitude α, the correlation function R and the geometric path delay δ [chips]. In case that no code multipath is considered ($R(\tau)=R(\tau-\delta)=1$), Eq. 13 simplifies to the well-known expression (e.g. Georgiadou and Kleusberg 1988 or Misra and Enge 2001):

$$\tan \theta = \frac{\alpha \sin \phi}{1 + \alpha \cos \phi} \tag{14}$$

The carrier multipath performance for the GPS L1 and the Galileo C-Band signal is illustrated in Fig. 15. For these diagrams, a multipath relative amplitude of $\alpha=0.5$ was assumed; all other parameters are according to Table 1.

When expressed in [m], carrier multipath is directly proportional to the carrier wavelength λ. As a result, the maximum phase errors caused by carrier multipath are significantly smaller at C-Band (by a factor of 3.2 compared to L1 and a factor of 4 compared to L2). This statement is strictly true only in the case of identical signal structure for both signals (i.e. identical modulation scheme and signal bandwidth) and can be roughly confirmed by Fig. 15. Furthermore, due to its much shorter code chip length compared to the GPS L1 signal, the C-Band signal is less susceptible to long-delay multipath (see Fig. 15). It can be shown that the maximum phase error (for $\alpha=1$ and in the case of infinite signal bandwidth) due to carrier multipath is $\theta=\pi/2$ corresponding to a carrier wavelength of $\lambda/4$ (e.g. Georgiadou and Kleusberg 1988 or Misra and Enge 2001). In this case, the maximum phase errors are 4.8 and 6.0 cm for the GPS L1 and the GPS L2 signal, respectively, and only 1.5 cm at C-Band.

Carrier smoothing at C-Band

The smoothing process combines code and phase measurements, so that the (noisy) pseudoranges can be smoothed and the influence of code noise can be significantly reduced (Hatch 1982). Additionally, carrier smoothing can be used to smooth out multipath effects. The use of C-Band frequencies allows significantly longer smoothing constants than at L-Band because of the reduced ionospheric code-carrier divergence at C-Band (factor 10). In this case, carrier smoothing at C-Band will be more accurate. Additionally, the frequency of multipath variations depends on the carrier frequency. Thus, it will be much higher at C-Band than at L-Band (factor of 3). As a result, it will be easier to smooth out the effects of multipath. Figure 16 illustrates a carrier smoothing simulation for both L-Band and C-Band. At both bands, identical smoothing constants and multipath amplitudes are assumed. Carrier smoothing at C-Band leads to significantly better results than at L-Band, i.e. the reduction of C-Band multipath by means of carrier smoothing is thus more effective than at L-Band.

Summary

Table 7 summarizes the signal tracking performance at L- and at C-Band. Benefits with respect to the other frequency band are indicated by "+" whereas drawbacks are indicated by "−". Note that the classification in Table 7 is only valid in the case where identical conditions are assumed in both bands (identical signal structure, C/N_0, smoothing constants,...).

Impact on satellite payload

Required satellite antenna input power

The main signal propagation parameter that affects the payload design is signal attenuation. Compared to the L-Band, free space loss and rain attenuation are significantly higher at C-Band. In order to compensate for the increased signal attenuation, a future C-Band signal will have to be much stronger (increased transmit power) than an equivalent L-Band signal. In other words, if we assume identical satellite transmit power at L- and at C-Band, the received C-Band signal will be much weaker.

The following computation of the minimum transmit power is based on the assumption that the power level of a

Table 7
Signal tracking performance at L- and at C-Band

Parameter	L	C
DLL tracking performance	o	o
PLL tracking performance	+	−
Code noise	o	o
Phase noise	−	+
Code multipath	o	o
Phase multipath	−	+
Carrier smoothing efficiency	−	+

Table 8
Computation of required minimum satellite antenna input power (C-Band vs. L-Band payload)

Link budget parameter	L-Band	C-Band
Received power level	−163 dBW	−163 dBW
Total sign. attenuation	189.3 dB	204.8 dB
Gain satellite antenna	14 dB	14 dB
Gain user antenna	0 dB	0 dB
Required satellite antenna input power	12.3 dBW / 17.0 W	27.8 dBW / 602.6 W

See Table 9 for details

Table 9
Required satellite antenna input power to provide a C/N_0 of 45 dBHz within the receiver tracking loops

Link budget parameter	Unit	GPS $L1$	C
Effective C/N_0 (tracking loop)	dBHz	45	45
Implementation loss	dB	6	6
C/N_0 @ user antenna output	dBHz	51	51
Power level (user ant. output)	dBW	−153	−153
Gain of user antenna	dBic	3	3
Power level (user ant. input)	dBW	−156	−156
Depointing loss (user)	dB	0.25	0.25
Polarization mismatch loss	dB	3	3
Tropospheric attenuation	dB	0.4	5.9
Free space loss (E=10°)	dB	185.4	195.4
Depointing loss (satellite)	dB	0.25	0.25
EIRP	dBW	33.3	48.8
Gain of satellite antenna	dBic	14.0	14.0
Required satellite antenna input power	dBW / W	19.3 / 85.1	34.8 / 3,020.0

Includes rainfall attenuation and attenuation due to clouds, fog, water vapor and oxygen

future C-Band signal for a 0 dBic antenna is −163 dBW (Ebner 2000). Assuming that the noise density is N_0=−204 dBW/Hz, the corresponding C/N_0 is 41 dB-Hz. The results are summarized in Table 8. There, the use of a 0dBic user antenna is assumed.

Normally, the specified received power level is much higher to provide a good $(C/N_0)_{eff}$ within the tracking loops. The following computation is based on the requirement that the signal should be tracked with a C/N_0 of at least 45 dBHz, a value that is easily obtained for GPS signals. The computation of the required satellite antenna input power is illustrated in Table 9. The following parameters were used:

– Receiver implementation loss: L=6 dB (low-end)
– Maximum atmospheric attenuation
– Gain of user antenna: 3 dB
– Gain of satellite antenna: 14 dB.

To provide an effective C/N_0 of 45 dB-Hz, the satellite antenna input power at C-Band will have to be approximately 35 times higher than at L-Band. Note, however, that the computed values are the result of a worst case analysis. The actual required satellite antenna input power strongly depends on the receiver quality (implementation loss), the type of user antenna (phased array vs. omni directional)
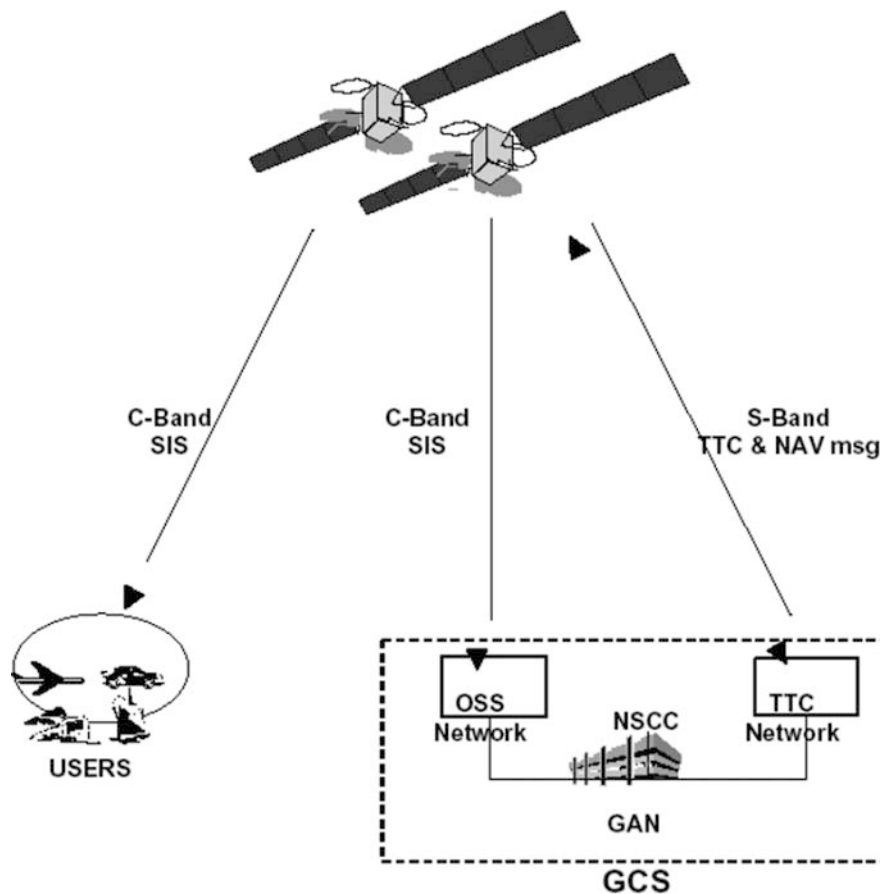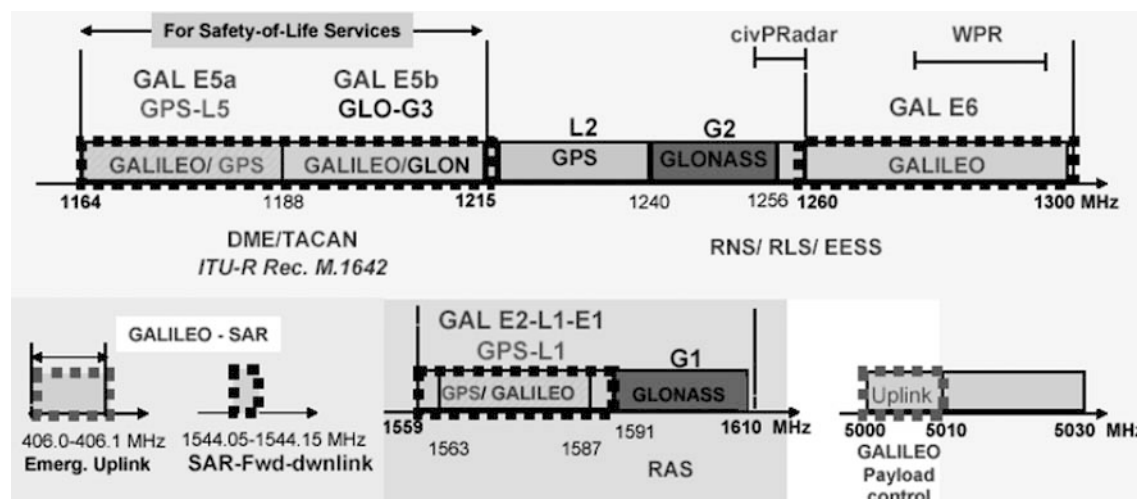
Fig. 18
C-Band high-level impact on a future Galileo mission. In this case
C-Band could be used for the generation and dissemination of
navigation signals. *OSS* orbit and synchronization station, *GAN*
global area network, *GCS* ground control segment, *NSCC* navigation
system control centre

and the actual atmospheric attenuation. Whichever sce-
nario is assumed, the required satellite antenna input
power at C-Band will be significantly higher than at
L-Band (assuming identical conditions at both bands).

C-Band payload characteristics

C-Band satellite payload configuration and accommodation

Galileo will transmit its services on several L-Band fre-
quencies (see Fig. 17). The C-Band could be used for safety
of life or public regulated services (PRS). Figure 17 gives
an overview of the GNSS frequency plan and the submitted
C-Band frequency (Galileo Industries 2003). Figure 18
illustrates the high-level impact on Galileo (Lindenthal
et al. 2001). However, in a future 2nd generation Galileo

mission it could be imaginable to use the C-Band also for navigation data calculation and dissemination.

The generation of the C-Band signal on board the GalileoSat spacecraft requires modifications in several areas of the spacecraft design. In particular, the payload and TT&C designs must be changed to provide the C-Band functions. On the other hand, these changes impact other areas of the spacecraft design like structure- and thermal subsystems and the electrical power subsystem. The satellite payload architecture has to meet the functional requirements of the C-Band payload. Four areas where modification of the existing design will be necessary have been identified:

— Signal generation subsystem
— Radio frequency (RF) subsystem
— Antenna subsystem
— Telemetry, tracking and command (TTC) subsystem.

For these subsystems, additional equipment has to be implemented to provide the C-Band SIS downlink and to facilitate the reception of uplinked information. Whilst the proposed architecture supports the objective of introducing a degree of independence from the L-Band payload and minimizes the necessary changes to the baseline design, it will however significantly increase the mass and power consumption of the payload.

The size of the payload is given by the type and amount of amplifiers which is a result of the C-Band link budget. The analyses have been performed for two atmospheric scenarios, considering atmospheric losses of 1.5 dB and 5.1 dB. An attenuation of 1.5 dB includes rain attenuation in the tropics with a 99.9% SIS availability and elevation angles of 10° (conservative approach) (Hegarty and Kim 1998;Saggese 2000). An attenuation of 5.1 dB considers rain attenuation in the tropics assuming 99.999% availability (worst case approach).

Signal generation

The signal generation subsystem will generate the low-power C-Band navigation signal from the uplinked navigation and integrity data supplied by the TT&C subsystem, before passing it to the RF subsystem for transmission to ground via the C-Band antenna. This subsystem will therefore also require a frequency generator unit and an upconverter capable of producing a signal at the required C-Band frequency. Additionally, it must have the capability to provide encryption. The functionality of the subsystem is assumed to be similar to that of the L-band navigation payload. Encryption of both data and spreading code is envisaged although the exact implementation of the encryption unit will strongly depend on the required level of security. The latter point will also drive the architecture in terms of independence from the L-Band payload. It is assumed that all functions for the provision of the C-Band base band signals are implemented in an external box to the L-Band system.

The RF subsystem will amplify the navigation message by means of high power Amplifiers (HPAs) and pass it to the antenna via an output filter. Coaxial input and waveguide output transfer switches will provide 2 for 1 redundancy

for the HPAs. The operating frequency and RF power levels (157 W) will require the use of travelling wave tube amplifiers (TWTA) rather than solid state power amplifiers (SSPA). The TWTA performs high efficiency power amplification to meet the C-Band equivalent isotropic radiated power (EIRP) requirements (35 dBW). Each of the two units comprises the travelling wave tube (TWT) and electric power conditioner (EPC). The use of only one active transmitting channel requires a single output filter to reject spurious signals generated by the payload and to ensure compliance with isolation for radio astronomy bands at 5,000 GHz. The filter will be centered at 5,019.87 MHz and will provide signal rejection in order to meet the C-Band out-of-band requirement and provide definition for the transmit pass band. The filter will be passive and non-redundant. The C-Band filter will be designed for high power handling and may require an additional harmonic filter to meet far out-of-band rejection requirements.

Antenna subsystem

The antenna transmits the amplified C-Band signal to the ground. This will require a separate C-Band antenna. Two options are possible, an independent C-Band antenna or one integrated C/L-Band unit in order to minimize the spatial separation of their phase centers. Each option has significant implications on mass and payload RF transmission power and the baseline chosen at present is to use a separate antenna. The C-Band antenna is a planar antenna using 42 patches as radiators placed on a circular antenna of 0.35 m diameter. The beam forming network (BFN) is located on the rear side of the radiating panel and the patches are fed by means of soldered pins. The antenna provides an iso-flux pattern gain of 15 dBi and could be accommodated – with appropriate redesign – on the existing L-Band antenna (if necessary).

Telemetry, tracking and command (TT&C) subsystem

The navigation data will be uplinked as a code division multiple access (CDMA) signal and thus requires a spread spectrum receiver on the spacecraft. For redundancy reasons, two separate receivers will be provided. These receivers will be independent to the TT&C and Integrity receivers although they will use the same antennas as the TT&C Subsystem. The receivers could be derived from the proposed design for the Integrity receivers. The proposed architecture tries to optimize the autonomy of the C-Band and L-Band payload with minimum changes of the payload design. All changes have an impact on satellite design (structure, thermal) and power.

Accommodation of the C-Band payload

The accommodation of the C-Band payload as an additional sub-element on GalileoSat considers the mass distribution and thermal concept of the satellite, the requirements for the harness interface between TWTA and C-Band antenna ("direct connections"), and the modular
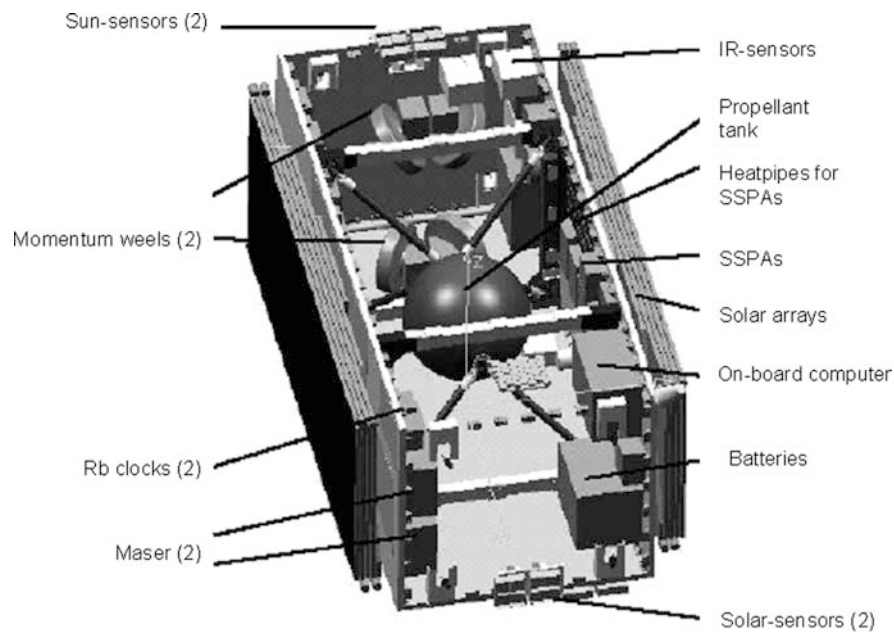
Fig. 19
GalileoSat with L-Band payload. *IR* infra red, *Rb* rubidium, *in brackets* number of units
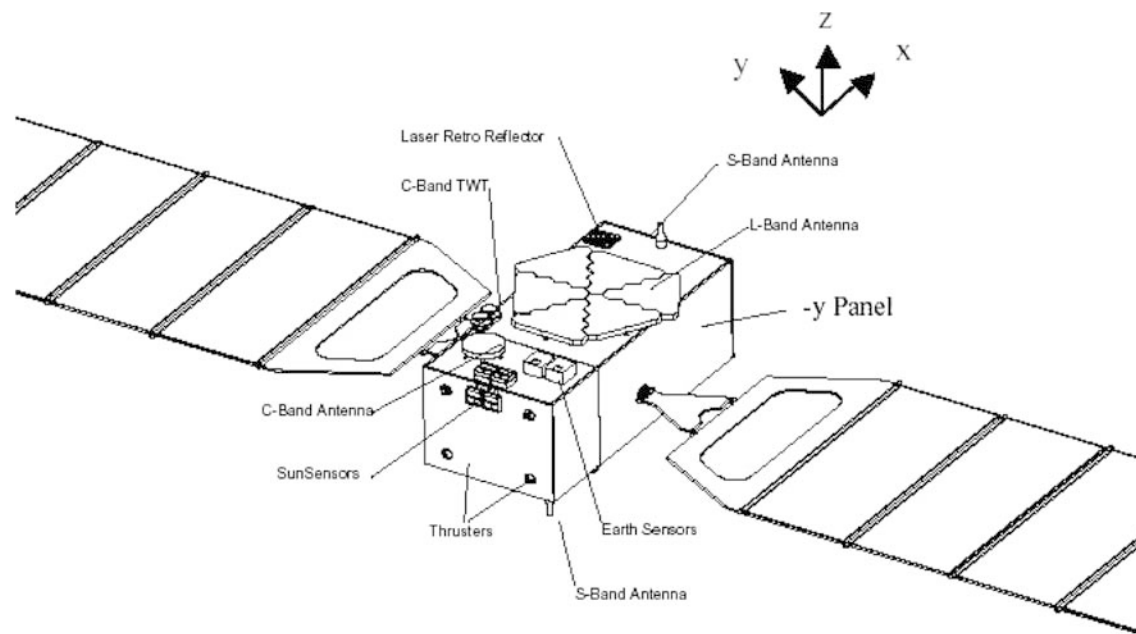

Fig. 20
GalileoSat with L- and C-Band payload (Lindenthal et al. 2001)

concept which allows a pre-integration of the payload. The modular concept of the satellite will be not changed, i.e. the C-Band payload will be integrated within the L-Band payload module. Units which strongly emit due to high thermal loss will be mounted close to the outer walls (Fig. 19). TWTAs will need their own radiator and heat pipes for heat minimization. The following elements have to be integrated: C-Band signal generator and processor, C-Band TT&C (2 units, one switched on, one cold redundant), TWT (2 units, one switched on, one cold redundant), EPC (2 units, one switched on, one cold redundant), switch for changing to redundant units (1), filter

for reduction of jamming signals and for shelter of the Radio Astronomy band, Mission and Control (M&C) subsystem, power supply and C-Band antenna.
Figure 20 shows the satellite with the integrated C-Band payload. The disk-shaped C-Band payload antenna is located on the outer surface of the +Z panel. The two S-Band antennas have been relocated with respect to the Galileo baseline configuration. They are placed with their long axis normal to the +z and -z panel of the satellite to provide maximum coverage to earth and deep space. The accommodation of both the S-Band and C-Band antenna, provides unobstructed Field of View (FOV) for the satellite's sun sensors and earth sensors as well as adequate place to adjacent satellites. Hence, the accommodation allows enough place for multiple satellites within the PROTON fairing envelope. The PROTON launcher is an

Table 10
Power and mass budget of a C-Band payload, which is mounted on a Galileo satellite and uses together with the L-Band: RB clock, Maser and USO M&C

Subsystem	DC power (W)	Thermal dissipation (W)	Mass (kg)	Size (mm)
C-Band NavProcessor	20	20	2	250×150×150
Signal generator	5	5	1	180×120×50
Modulator	2	2	1	180×120×50
TWTA	250	130	TWT:2·1.1 EPC: 2·1.7	TWT (L=420, $ı$=150) EPC: 230×110×50
Filter		10	0.5	300×63.5×44.5
Antenna			2	$ı$=403, h=250
Wave guide		20	3	L=1,000
M	amp;C	10	10	2·4
Power supply	7.1	7.1	2×10	
Sum	294	204.1	43.1	

1 active unit and 1 cold redundant unit

example as it is the carrier with the smallest internal diameter, which can be used for a multi-satellite launch.

Integration of the C-Band subsystems on GalileoSat

For the integration, it has been considered that Rubidium (Rb) clocks and passive Hydrogen (H)-Masers are mounted in sufficient distance to the TWTAs, so that the magnetic field of the TWTAs does not disrupt the clocks. The mounting considers the mass distribution and the thermal requirements. The solid state amplifiers are mounted considering the same boundary conditions. The TWTAs are emitting 60% of their thermal losses through the outer walls. The remaining 40% are dissipated via heat pipes to the radiator, which they share with the four L-band SSPAs.

Budgets

Table 10 lists the mass- and power distribution of the GalileoSat C-Band payload, calculated for an atmospheric attenuation of 1.5 dB (case 1). The high power consumption of 250 W and the dissipation energy of 130 W compared to the output power of 120 W are remarkable. For case 2 (atmospheric attenuation 5.1 dB), the transmitting signal power has to be increased by a factor of 2.3, which means that a TWTA with a DC power of 575 W is required. The overall DC power increases from 294 to 619 W.
The maximum solar power available for a GalileoSat is 1,470 W (Lindenthal et al. 2001). For case 1 (atmospheric attenuation 1.5 dB, baseline) 1,450+294=1,744 W are required. This is 20% more than can be achieved by the GalileoSat solar panels. This power can be provided by 2 additional solar panels (silica cells, max. 2×1,000 W power) or a panel consisting of new silica solar cells with improved efficiency (1,900 W power). For case 2 (attenuation 5.1 dB worst case) 145+619=2,069 W are required. This is more than 43% than can be achieved with the proposed solar arrays. Additionally, larger solar panels are required to achieve the output power of 575 W. The impact on satellite design (mass, size, thermal) is significant, a redesign of the satellite would be necessary as the C-Band payload then would be the driving force. For case 1, Table 10 gives an overview over the required power, thermal dissipation and mass budget of the C-Band payload which is accommodated on a GalileoSat and together with L-Band uses the Rb clock, H-Maser and Ultra Stable Oscillator (USO) M&C Processor.

The overall mass of GalileoSat including the L-Band payload amounts to 665 kg. Together with the integration of a C-Band payload the mass increases by 30 kg (two additional solar arrays) and 7 kg by an additional battery. Hence, the total mass amounts to around 745 kg with additional solar panels and about 715 kg with new panels. The impact of the additional mass on the satellite (frequencies, dispenser, Attitude Orbit and Control System (AOCS), propellant and launcher (design, stiffness) has to be analyzed in another study.

Summary

The accommodation analysis shows that the C-band payload can be integrated on a GalileoSat if realistic constraints are assumed for the link budget (e.g. an atmospheric attenuation of 1.5 dB). For the C-Band signal generator, additional TT&C channels, C-Band antenna and a better TWTA amplifier are needed. Beneath additional subsystems and mass additional or solar arrays with a better efficiency are required. The impact of the C-Band payload on the satellite structure, AOCS, thermal aspects, launcher has to be investigated in an additional study. For the case atmospheric attenuation=5.1 dB the power, size and mass increase of the C-Band payload is so large that it dominates the whole satellite.

Impact on future C-Band receivers

Enhancing the poor PLL performance

As it has been shown above, the PLL performance at C-Band is much poorer than at L-Band (see Fig. 11). It is therefore of importance to find suitable approaches to enhance the PLL performance at C-Band. The following approaches can be taken into account.
Enhancement of the reference oscillator's g-sensitivity. The influence of random vibration strongly depends on the oscillator's g-sensitivity. The resulting phase jitter is directly proportional to the oscillator's g-sensitivity so that a reduction of this parameter results in less phase jitter

(Irsigler and Eissfeller 2002). Random vibration is an issue especially for kinematic applications, whereas such influences are not present in static applications. The main drawback of this approach is that such optimized oscillators are more expensive than standard temperature compensated crystal oscillators (TCXOs) due to the more stringent requirements.

Use of high stability reference oscillators. The oscillator's frequency instability can be described by its Allan deviation. As is the case for random vibration, frequency instabilities also result in phase jitter. In order to reduce the resulting phase errors, the use of a high stable reference oscillator (e.g. an oven controlled crystal oscillator, OCXO) instead of a standard TCXO should be taken into account. The main drawbacks of this approach are increased cost and power consumption compared to a standard TCXO. Additionally, the influence of frequency instabilities also depends on the loop noise bandwidth. A reduction of the resulting phase jitter can principally be achieved by increase of this bandwidth. However, the resulting enhancements with respect to oscillator phase noise are marginal and by increasing the loop noise bandwidth, the thermal noise increases correspondingly.

Significant increase of the loop noise bandwidth. The dynamic stress error strongly depends on the loop noise bandwidth. The smaller the loop noise bandwidth, the harder to track the signal dynamics. On the other hand, increase of the loop noise bandwidth reduces the influence of dynamic stress and is therefore a possible approach to enhance the PLL performance. The main drawback of this approach is that by increasing the loop noise bandwidth, thermal noise also increases.

PLL design at C-Band. To ensure robust carrier phase tracking at C-Band, the following PLL implementations should be taken into account:

- Use of third-order PLL (a second-order PLL at C-Band would only be stable in static applications).
- Slight increase of the loop noise bandwidth compared to the L-Band (e.g. B_L=20 Hz) for static and low dynamics applications.
- Significant increase of the loop noise bandwidth compared to the L-Band (e.g. B_L=40 Hz or even higher) for applications with high signal dynamics.
- Use of high quality oscillators with low g-sensitivity (e.g. screened OCXOs) and/or special oscillator mounting techniques which are able to absorb occurring vibrations.

Possible approaches to achieve sufficient high signal power levels at C-Band

Due to the increased free space loss and tropospheric attenuation, a future C-Band signal will be approximately 10–16 dB weaker than an L-Band signal when received at the ground (assuming identical satellite transmit power and identical user antennas). Signal strength at the user antenna also determines the $(C/N_0)_{eff}$ with which the signal is tracked within the tracking loops. Two general approaches can be considered to compensate for the 10–16 dB loss at C-Band:

increase of satellite transmit power and suitable antenna/receiver design. To achieve sufficient high $(C/N_0)_{eff}$ at C-Band without significantly increasing the satellite transmit power, the following approaches can be used:

Use of phased array antennas. In contrast to standard omni directional user antennas, phased array antennas consist of multiple antenna elements which are arranged in the form of an array. A prototype C-Band antenna has been developed by the Institute of Communication and Navigation of the German aerospace center (DLR). The antenna consists of 25 antenna elements (5×5 array) and by means of digital beam forming, up to six beams can be generated allowing simultaneous tracking of up to six satellites. The beam width depends on the number of antenna elements, e.g. for the discussed 5×5 array, the half power beam width is about 30°. By means of these relatively narrow beams, a gain of approximately 10 dBic can be achieved. Compared to a 3 dBic standard omni-directional user antenna, the received power level is increased by 7 dB. Thus, the use of phased array antennas is principally a suitable approach to (partially) compensate for the increased free space loss at C-Band. It is also a suitable approach to null out multipath and/or interfering/jamming signals. On the other hand, however, the use of such antennas result in additional drawbacks which are discussed later on.

Minimization of receiver implementation losses. As can be derived from Table 9, the effective C/N_0 also depends on the receiver implementation loss. Since the C/N_0 of the received C-Band signal will be much lower than an equivalent L-Band signal (assuming identical conditions), no more additional losses can be accepted. In Table 9, an implementation loss of 6 dB has been assumed. This is a typical value for low-end receivers. In high-quality receivers, implementation losses of 1–2 dB can be expected. Especially at C-Band, the implementation losses should be as small as possible. The main parameters that determine the receiver implementation loss is the LNA (low noise amplifier) noise figure and the quantization process of the A/D conversion. As can be derived from Parkinson and Spilker (1996), the quantization process causes signal degradation. This degradation strongly depends on the resolution of the quantization process and it can be shown that the actual signal degradation decreases with increasing resolution. As a result, a minimum of 2 bit is required to limit the signal degradation to 1–1.5 dB. The use of 3–5 bit quantization can reduce the corresponding signal degradation down to 0.5–0.7 dB (Parkinson and Spilker 1996). As a result, multi-bit quantization is strongly recommended for future C-Band receivers.

Discussion

Increased transmit power vs. phased array antenna

The use of phased array user antennas and the construction of high-end C-Band receivers with very low implementation losses may not be necessary if the satellite antenna input power is significantly increased. In the following, both approaches (increase of satellite
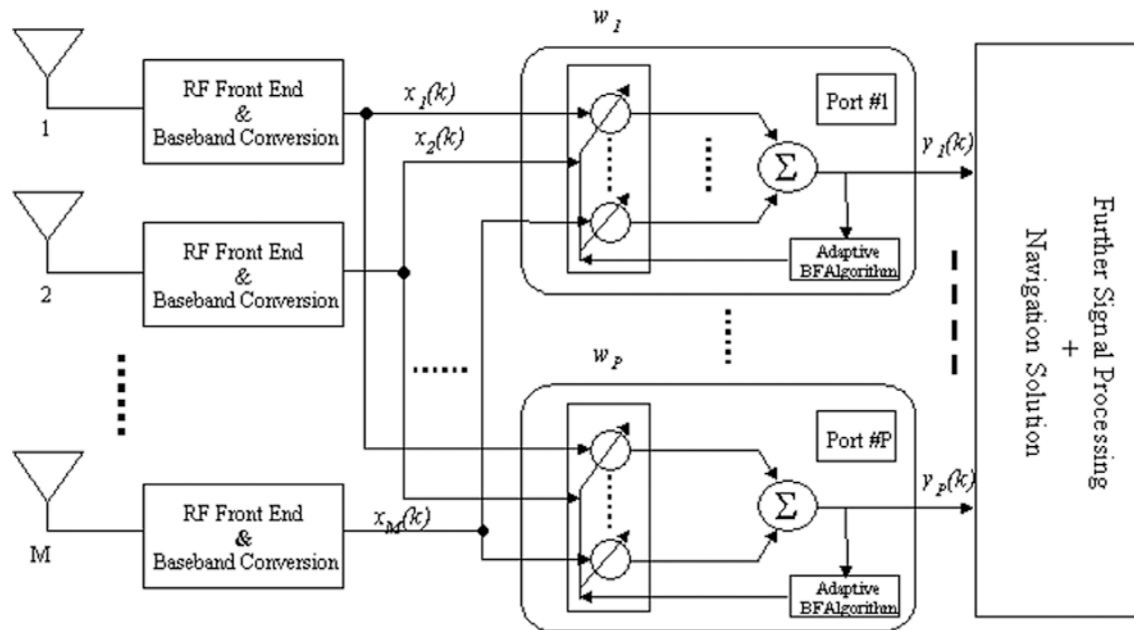
Fig. 21
Block diagram of an integrated receiver unit utilizing a phased array antenna with digital beam forming (*BF*)

transmit power and use of phased array antennas) are discussed with respect to their benefits and drawbacks. *Increase of satellite transmit power.* Many drawbacks of C-Band navigation could be compensated by increasing the satellite transmit power by 10 dB (minimum). By means of this approach, the following enhancements can be achieved:

– Compensation of the increased free space loss.
– Increase of $(C/N_0)_{eff}$ within the tracking loops, thereby reducing the influence of thermal noise, the cycle-slip probability and enhancing the DLL/PLL performance.
– Compensation of the increased tropospheric attenuation, thereby increasing availability.
– Use of omni-directional user antennas, resulting in a relatively simple receiver architecture, moderate power consumption, low manufacturing costs and enhanced mass-market suitability.
– Less attention must be paid to the development of high-quality C-Band receivers with low implementation losses, so that simple low-end C-Band receivers using simple 1 bit-quantization techniques are feasible.

However, increase of the satellite transmit power results in additional problems:

– Increased power consumption (satellite).
– Necessity of additional and/or larger solar panels.
– More space required within the satellite-launching rocket.
– Increased weight of the satellite-launching rocket.
– Increased launch cost.

Use of phased array antennas. At first sight, the use of phased array antennas seems to be a suitable approach to limit the required satellite transmit power and to compensate the occurring signal losses at C-Band. The main advantages of this approach are the increased antenna gain compared to an omni-directional antenna and the ability to null out multipath and/or interfering/jamming signals by means of beam forming. However, the use of such antennas results in the following drawbacks:

– Phased array antennas will presumably be larger, heavier, and more unwieldy and complex than omni-directional antennas. Due to their increased size, they will not be suitable for certain applications (e.g. in case very small receivers are needed).
– Since a phased array antenna consists of several antenna elements, a corresponding amount of front ends will be necessary (one front-end per antenna element). Additionally, a beam-forming and beam-steering unit will have to be implemented (see Fig. 21). In contrast to an omni-directional receiver, the phased array approach thus results in a complex receiver architecture, thereby increasing size, weight, power consumption and manufacturing cost.

Conclusion

C-Band navigation offers both benefits and drawbacks. Although it might be feasible to overcome the technical issues, it is uncertain that a (future) C-Band navigation system can compete with current sophisticated L-Band equipment. Furthermore, the L-Band performance will be permanently upgraded in the near future (GPS modernization, Galileo L-Band). Therefore, satisfactory acceptance of a C-Band system by the SatNav community is doubtful. However, a future C-Band signal might be an interesting option in combination with L-Band signals. Moreover, technological progress might balance some of the disad-

vantages and might allow C-Band navigation within a future generation of Galileo.

Biographies

Markus Irsigler is research associate at the Institute of Geodesy and Navigation at the University of the Federal Armed Forces Munich. He received his diploma in Geodesy and Geomatics from the University of Stuttgart, Germany. His scientific research work focuses—among other topics—on overall GNSS receiver performance and multipath mitigation.

Günter W. Hein is Full Professor and Director of the Institute of Geodesy and Navigation at the University FAF Munich. He is responsible for research and teaching in the fields of high-precision GPS/GLONASS/GNSS positioning, navigation, physical geodesy, gravimetry and satellite geodesy. He has been working in the field of GPS since 1984 and is author of numerous papers on kinematic positioning and navigation as well as sensor integration. In 2002, he received the "Johannes Kepler Award" from the Institute of Navigation (ION) for "sustained and significant contributions to satellite navigation".

Andreas Schmitz-Peiffer received his Master and PhD in Atmospheric Physics at the University of Kiel, Germany. From 1986 to 1989, he worked at the Institute for Atmospheric Sciences of the German Aerospace Center in the field of lidar systems. His current work at Astrium GmbH focuses on the development of the future European satellite navigation system Galileo.

References

Ebner H (2000) Galileo overall architecture definition: SIS Frequency Characteristics, GALA-ASTR-DD-019, issue 5.0, 15.11.2000

European Radiocommunications Office (2000) The world radio-communication conference 2000: main issues, European and other regional positions, Results (Final Report), July 2000

Galileo Industries (2003) Galileo Phase B2 Study Final Presentation, ESTEC, 11.07.2003

Georgiadou Y, Kleusberg A (1988) On carrier signal multipath effects in relative GPS positioning. Manuscripta Geodaetica 13:172–179

Goldhirsch J, Vogel W (1998) Handbook of propagation effects for vehicular and personal mobile satellite systems. John Hopkins University and University of Texas

Hatch R (1982) The synergism of GPS code and carrier measurements. In: Proceedings of the 3rd international geodetic symposium on satellite Doppler positioning, vol 2, pp 1213–1231

Hegarty C, Kim T (1998) Assessment of the use of C-Band for the second civil GPS frequency; MITRE CAASD, 23.07.1998

Irsigler M, Eissfeller B (2002) PLL tracking performance in the presence of oscillator phase noise. GPS Solutions, vol 5, issue 4. Wiley Periodicals Inc.

Itu-R (1994) Propagation and prediction methods required for the design of earth-space telecommunication systems. ITU-R Recommendation PN.818–3

Kajiwara A (2000) Foliage attenuation characteristics for LMDS radio channel. IEICE Trans Commun E83-B(9)

Kaplan ED (1996) Understanding GPS, principles and applications. Mobile Communications Series. Artech House, Norwood

Liebe HJ (1989) MPM: an atmospheric millimeter wave propagation model. Int J Infra Milli Waves 10(6) S. 631–S. 650

Lindenthal W et al (2001) GalileoSat, C-Band navigation payload space segment assessments, WP 3300, Astrium, 19.01.01

Maral G, Bousquet M (1999) Satellite communications systems: systems, techniques and technology, 3rd edn. Wiley, Chichester

Millman GH (1970) Tropospheric effects on space communications. In: Agard conference proceedings No. 70 on tropospheric radio wave propagation, Part 1, pp S. 4-1–S. 4-29

Misra P, Enge P (2001) Global positioning system: signals, measurements and performance. Ganga-Jamuna Press, Lincoln

Parkinson BW, Spilker JJ (1996) Global positioning system: theory and applications, vol I, Progress in astronautics and aeronautics, vol 163, American Institute of Aeronautics and Astronautics, Inc., Washington

Saggese E (2000) C-Band GAS: system architecture definition and analysis. GalileoSat definition study, WP 3100, Alenia Spazio S.p.A., 19.12.2000

Van Dierendonck AJ, Fenton P, Ford T (1992) Theory and performance of narrow correlator spacing in a GPS receiver. Navigation 39:265–283

Van Dierendonck AJ, Klobuchar J, Quyen Hua (1993) Ionospheric scintillation monitoring using commercial single frequency C/A code receivers. In: Proceedings of ION GPS-93, Salt Lake City, pp 1333–1342